Molecular Functions of Conserved Developmentally-Regulated GTP-Binding Protein Drg1 in Translation

Fuxing Zeng, Melissa Pires-Alves, Christopher W. Hawk, Xin Chen and Hong Jin*

*Corresponding author

Address:

Department of Biochemistry
Center for Biophysics and Quantitative Biology
University of Illinois at Urbana-Champaign
600 S. Mathews Avenue, Urbana, IL 61801

Phone: (217)244-9493

Fax: (217)244-5858

Email: hjin@illinois.edu

SUMMARY

Developmentally-regulated GTP-binding (Drg) proteins are important for embryonic development, cell growth, proliferation, and differentiation. Despite their highly conserved nature, the functions of Drg proteins in translation are unknown. Here, we demonstrate the yeast Drg ortholog, Rbg1, alleviates ribosome pausing at Arginine/Lysine-rich regions in mRNAs, and mainly targets genes related to ribonucleoprotein complex biogenesis and non-coding RNA processing pathways. Furthermore, we reveal the global architecture of the ribosome and the molecular interactions involved when Rbg1 and its binding partner, Tma46, associate with the ribosome using biochemistry and single particle reconstruction using cryoEM. Our data show that Rbg1/Tma46 associate with the larger subunit of ribosome via the N-terminal zinc finger domain in Tma46, and that the protein complex helps to enrich translating ribosomes in the post-peptidyl transfer state, after peptide-bond formation, but before elongation factor binding and tRNA translocation. Based on our results and the conserved nature of Drg proteins, broader functions of the Drg proteins in the protein synthesis and quality control pathways of eukaryotic cells are proposed.

INTRODUCTION

The highly conserved, developmentally-regulated GTP-binding proteins (Drg) play important roles in cellular processes such as embryonic development, cellular differentiation, and proliferation. Drg was originally identified as a so-called NPC-Expressed, Developmentally Down-regulated (NEDD)-3 gene. mRNA of the NEDD-3 gene was identified to be highly expressed in neural precursor cells in the developing mouse brain [1]. Shortly after its discovery, Drg mRNA and protein were found to be widely expressed at variable levels in cultured cells, as well as other embryonic, postnatal, and adult murine tissues [2]. The coding sequence of mouse Drg1 contains a canonical G motif common to the GTPase superfamily [3]. Genes homologous to mouse Drg have been found in a variety of species and tissues. A subsequent phylogenetic study revealed that eukaryotes typically contain two Drg genes, Drg1 and Drg2, whereas archaea only contain one [4]. The amino acid sequences of Drg1 and Drg2 are highly homologous to each other, especially in their G domains, which are characterized by the five known G-motifs, as well as in their C-terminal TGS (Threoyl-tRNA synthetase ThrRS, GTPase and SpoT) domain (**Supplemental Figure 1**). Furthermore, distributions of the steady-state mRNA levels of Drg1 and Drg2 are fairly similar across different tissues in Xenopus [5], murine, and human cells [4].

Expression of Drg proteins is controlled by Drg family regulatory proteins (Dfrp) through direct physical associations: Dfrp1 specifically binds Drg1, whereas Dfrp2 binds to Drg2 preferentially [6]. Similar to the Drg proteins, Dfrp proteins are highly conserved. Yeast and mammalian Dfrp proteins share a partially-conserved region of about 60 amino acids, the DFRP domain, which is critical for binding to Drg proteins (**Supplemental Figure 1)**. Strikingly similar spatial expression patterns of Drg1 and Dfrp1 mRNAs in Xenopus embryos and adult tissues were observed [6]. In addition, Drg1 and Dfrp1 proteins showed the same subcellular localization in HeLa S3 cells [6]. Importantly, association of Dfrp and Drg confers stability to the Drg protein in vivo [6] and enhances the GTPase activity of the Drg in vitro [7,8].

Drg1 proteins are highly expressed in actively growing and developing cells, as well as reproductive adult tissues of plants, animals, and humans. Consistent with their functions in growth control, cellular differentiation, and proliferation, altered Drg expression leads to cell transformation or cell cycle arrest [9-12]. Despite extensive studies, basic aspects of the role Drg proteins have in protein synthesis remain unknown. First, while high levels of Drg expression are positively correlated with their functions in translation, and both Drg1/Dfrp1 and Drg2/Dfrp2 complexes copurified with translation factors [13], molecular functions of these proteins in translation are not understood at all.

Second, the interactions between Drg1 with translation related factors, especially with the central translational machinery, the ribosome, are completely unknown. One of the isoforms, Drg1/Dfrp1, not Drg2/Dfrp2, associates with translating ribosomes [7,13-15]. The yeast Drg1, Dfrp1, Drg2, and Dfrp2 orthologs are Rbg1 (Ribosome-binding GTPase 1), Tma46 (Translation machinery associated 46KDa protein), Rbg2, and Gir2, respectively [15-17]. X-ray crystal structures of isolated Rbg1 with a truncated Tma46, containing amino acid residues 205 through 345, but lacking the zinc finger region (Tma46-ΔZnF, **Supplemental Figure 1**), showed that the helix-turn-helix (HTH), S5D2L, and TGS domains buttress the G domain of Rbg1, whereas Tma46-ΔZnF, composed of multiple α-helical regions, adopts an extended conformation and binds to Rbg1 via its G and TGS domains [7]. However, nucleotides such as GTP or GDP are not present in the structure. Not only is its ribosome interaction more complex, but the overall

conformation of the heterodimer merits consideration of how nucleotide-binding contributes its recruitment in the translation function.

Here, using yeast as a model system, we demonstrate that the yeast Drg1 ortholog, Rbg1, alleviates ribosome pausing at Arginine/Lysine-rich regions in mRNAs and impacts translation of cellular mRNAs functionally related to the ribonucleoprotein complex biogenesis and non-coding RNA processing pathways. Furthermore, the cryoEM reconstruction of the native Rbg1-translation complex provided the first structure of Rbg1/Tma46-ribosome engaged in translation. These findings have functional implications for the mechanism of translation regulation in the R/K-rich sequences in eukaryotic cells.

RESULTS

1. Rbg1 depletion results in translation pausing at certain amino acids.

To study the functions of Rbg1 specifically, we first deleted the rbg1 gene, thus creating the Δrbg1 strain. Consistent with the earlier observation that Δrbg1strains showed no observable growth defects [13], we detected no obvious changes to the ribosome protected regions using ribosome profiling experiments (Jin Lab, unpublished data).

To more effectively capture and compare ribosome dynamics *in vivo* at both a genome-wide scale and in a drug-free way, we employed the 5PSeq methodology (**Supplemental Figure 2A and 2B**), which captures 5' monophosphate (5P) mRNA intermediates, produced by 5' exonucleases (such as Xrn1 in yeast) that follow the last translating ribosome on an mRNA [18]. As a result, 5PSeq enriches ribosome footprints on the mRNA undergoing 5' to 3' co-translational degradation, providing a sensitive measure of ribosome dynamics in translation and quality control pathways. Using this method, we observe translation pausing when the ribosome translates certain amino acids, such as Arginine and Lysine (**Figure 1A**). Considering that the length of ribosomal footprints from the ribosomal A, P, and E-sites to its protected 5'-end is 17nt, 14 nt, and 11nt in this experiment (**Supplementary Figure 2C**), it is clear that the observed pausing in the translating ribosome occurs at the amino acid level rather than at the nucleotide level.

Consistent with our observations at the genomic level, our cell growth assay in the presence of anisomycin demonstrated that Rbg1 alleviates ribosome stalling. The antibiotic anisomycin binds to the peptidyl transferase center (PTC) of the ribosome and causes translational stalling [19]. In the presence of 10 μg/ml anisomycin, Rbg1 deletion resulted in slight, but observably slower growth of yeast cells on YEPD plates (**Figure 1B**). Addition of Rbg1 proteins in Δrbg1 cells alleviated this growth defect (**Figure 1B**), suggesting that Rbg1 indeed helps to resolve paused ribosomes in the cell.

2. Functional inactivation of Rbg1, Rbg2, and Slh1 leads to accumulation of ribosomes at the start codon.

To further understand this phenomenon, we created multiple knockouts of genes functionally related to rbg1. Results from yeast genetic screens showed that yeast Rbg1, Rbg2, and Ski2-like helicase 1 (Slh1) are simultaneously required for efficient translation and cell growth [13]. Slh1 is another highly conserved eukaryotic protein that associates with translating

ribosomes in eukaryotes [13]. Therefore, we created a conditional triple-knockout strain, Δrbg2Δslh1-Rbg1d, by simultaneously inhibiting Rbg1 mRNA transcription and promoting Rbg1 protein degradation [20,21] . This way, when combined with the single (Δrbg1) and double (Δrbg2Δslh1) knockouts, cellular functions of Rbg1 can be specifically targeted and accumulative functions of the three proteins, Rbg1, Rbg2, and Slh1 can also be studied (**Supplemental Figure 3A**).

Similar growth phenotype patterns were observed at 19, 30, and 37°C for the wild-type and mutant strains (**Supplemental Figure 3B**), suggesting the conditional knockout strain Δrbg1Δslh1-Rbg1d is valid, and the cellular function of Rbg1 is likely to be temperature-independent. Furthermore, a progressive decrease of polysomes and increase in 40S, 60S, and 80S ribosomal fractions is observed when cells depleted these three proteins one by one, demonstrating a gradual decrease of global translation among Δrbg1, Δrbg2Δslh1, and Δrbg2Δslh1-Rbg1d strains (**Supplemental Figure 3C**).

Using the 5P-Seq method, metagene analyses demonstrated progressively increasing peaks at the -14 nt and 4 nt positions in Δrbg1 (**Figure 1D**), Δrbg2Δslh1 (**Figure 1E**) and Δrbg2Δslh1-Rbg1d cells (**Figure 1F**, solid lines in blue) compared to the corresponding control (dotted lines in magenta). Since the length of ribosomal footprints from the ribosomal P-site to its protected 5'-end is 14 nt in this experiment, these two positions correspond to the ribosome pausing at the start codon and nascent peptide-induced ribosome pausing with seven amino acids in the exit tunnel after translation initiation, respectively (**Supplemental Figure 2C and 2D)**. Although ribosome pausing was observed at the start codon, no consensus sequences at the amino acid or nucleotide levels were found in this region (data not shown). By contrast, we found that ribosome pausing at the seventh amino acid was specifically associated with peptides containing a MSxxxxx pattern (**Supplemental Figure 4**), the same observation was reported earlier [18]. Finally, gene ontology analyses were carried out to identify pathways that are enriched with strong ribosome pausing at the start codon region, and results show that genes related to ribonucleoprotein complex biogenesis and non-coding RNA processing pathways are affected (**Figure 1G**), suggesting that the presence of these three proteins is important for translation of mRNAs involved in these pathways.

3. Deletion of Rbg1, Rbg2, and Slh1 causes redistribution and accumulation of ribosomes in the 5' end of mRNA.

The mRNA degradation machinery closely follows the last translating ribosome in 5PSeq, where the translation rate of the last ribosome affects the amount of 5P intermediates and their positions in the coding region of mRNA [18]. As a result, a 3-nt periodicity pattern of the 5P intermediates in the coding region (CDS) informs about ribosome dynamics, where a strong 3-nt periodicity pattern suggests a relatively slower rate of translation of the mRNA by the ribosome when compared to a weak 3-nt periodicity pattern (**Figure 2A)**. In wild type cells, it was suggested to be difficult for the exonuclease to catch up to the last translating ribosome near the start codon because decapping was rate-limiting [18]. Compared to those in the wild type (**Figure 1C**), Δrbg1 (**Figure 1D**), and Δrbg2Δslh1 cells (**Figure 1E**), we observe a much clearer 3-nt periodicity pattern of the 5P intermediates in the 5' end of coding regions in Δrbg2Δslh1-Rbg1d cells (**Figure 1F**), suggesting that the rate of translation elongation was significantly decreased when the cells lost the functions of Rbg1, Rbg2, and Slh1 simultaneously.

To characterize this phenomenon, we calculated the proportion of 5P reads in the ribosome-protected frame for each codon. The proportion score for a wild type control sample, lacking the characteristic 3-nt periodicity pattern, was estimated to be around 0.33. In agreement with an earlier observation [18], the proportion scores of 5P reads slowly increase from ~0.33 at the start codon to ~0.45 at the 300nt position in the ribosome-protected frame for the wild type cells (**Figure 2B-D, black lines**). In contrast, the proportion values at the same position of the mRNA increase slightly faster in the Δrbg1 (red line in **Figure 2B**) and Δrbg2Δslh1 cells (green line in **Figure 2C**). Most notably, this value increases to 0.45 immediately after the start codon in the Δrbg2Δslh1-Rbg1d cells (blue line in **Figure 2D**), suggesting an obvious decrease in the rate of elongation in these cells.

Genes with higher proportion values in the Δrbg2Δslh1-Rbg1d cells when compared to the wild type cells were extracted and subjected to further analysis. Unsurprisingly, gene ontology analysis results showed that these genes are enriched in pathways related to the biogenesis of ribonucleoprotein complexes, including ribosomes, as well as noncoding RNA processing (**Figure 2E**).

4. Rbg1 alleviates ribosome pausing at arginine/lysine-rich regions

To quantify elongation pausing and to determine which sequences resulted in ribosomal pausing, we calculated the pause score at each position as described, with modifications [22]. Consistent with our initial observation (**Figure 1A**), results show that ribosomes have a tendency to pause at the R-/K-rich sequences in all of the following mutant cells: Δrbg1, Δrbg2Δslh1 and Δrbg2Δslh1-Rbg1d (**Figure 3A and 3B**). In-line with these results, Slh1 was shown to alleviate the ribosomes stalled at arginine/lysine rich regions by facilitating ribosome-associated quality control[23].

5. Rbg1 binds to ribosomes in the classical state via the zinc-finger domain in Tma46

4A. The zinc finger domain in Tma46 is important for the ribosomal association of the Rbg1/Tma46 complex

How does the Rbg1/Tma46 heterodimer interact with the ribosome? Earlier studies showed that deletion of either the zinc finger domain in Tma46 or the TGS domain in Rbg1, as well as mutations in Rbg1's G domain which either compromise the nucleotide-binding or GTPase activity of the protein, failed to rescue the severe growth defect in the triple knockout Δrbg1Δrbg2Δslh1 cell [13]. Among these individual domains, the function of the zinc-finger domain in Tma46 is unclear. To study whether this domain mediates association of Rbg1/Tma46 to the ribosome, we deleted the zinc-finger domain, creating the Tma46-ΔZnF mutant protein; and used immunoblotting to characterize the ribosomal association capability of the Rbg1/Tma46-ΔZnF complex. As shown in **Figure 4A**, Rbg1/Tma46-ΔZnF does not associate with the ribosome (Top panel), whereas the wild type Rbg1/Tma46 complex does (Bottom panel). This suggests that the zinc-finger domain of Tma46, while not required for Rbg1/Tma46 heterodimer formation [7], is required for Rbg1/Tma46- ribosomal association.

4B. Rbg1/Tma46 mainly associates with the large ribosomal subunit.

To locate the binding site of Rbg1/Tma46 on the ribosome, a 6XHis tag was inserted into the C-terminal region of the Rbg1 protein, and the Rbg1/Tma46 bound 80S ribosomes were purified from micrococcal nuclease-treated polysome fractions. The resulting ribosomal complex was then incubated with 1.8 nm NTA-gold particles that bind to the His-tagged Rbg1 protein. Unbound NTA-gold particles were removed by gel filtration (**Supplemental Figure 5A**). As shown in **Figure 4B**, when compared to the unlabeled ribosomal complex (**Supplemental Figure 5B**), 2D classification results of the gold-labeled samples show a clear, bright spot, the gold signal, on the ribosome. The position of the gold particle is close to the ribosomal E-site, around the L1-stalk region [24]. Does the Rbg1/Tma46 complex bind directly to the L1-stalk? Using limited RNase I-treatment, under which most of the flexible regions on the ribosomal surface are removed (**Supplemental Figure 6**), including some of the L1-stalk and other rRNA expansion segments, the Rbg1/Tma46 complex nonetheless binds to the 80S ribosome. This suggests that the flexible RNA regions of L1-stalk, as well as other flexible rRNA regions on the surface of the ribosome are unlikely to significantly contribute to Rbg1/Tma46 ribosomal association.

4C. Binding of the Rbg1/Tma46 heterodimer enriches the ribosome in the post-peptidyl transfer state in translation.

Nucleotide binding and GTP hydrolysis are important for both Rbg1's association with the ribosome and its cellular functions [13]. Here, using a non-hydrolysable GTP analogue, GDPCP, we employ cryoEM to investigate the molecular architecture of the ribosome when the Rbg1/Tma46 heterodimer is bound. To prepare a sample amenable to structural studies, we inserted a 3XFLAG tag at the end of Rbg1 gene of the yeast chromosome. Native Rbg1/Tma46-ribosome complexes were purified from cellular ribosomal fractions using affinity pulldown of the 3XFLAG epitope tag. This method allows us to comprehensively sample physiologically-relevant functional states of the ribosome when the protein complex binds. Ribosomal fractions used for structural studies were not treated with nucleases. Using this method, 6725 micrographs were collected on the sample, and after rounds of 2D and 3D classifications, 209,143 ribosomal particles were selected for single particle reconstruction analysis. A more detailed experimental procedure is outlined in **Supplemental Figure 7**.

As shown in **Figure 4C**, the conformation found in the Rbg1/Tma46-enriched ribosomes is distinct from that of the un-enriched ribosomes undergoing translation. Nascent peptides in the Rbg1/Tma46-enriched ribosomes are attached to the CCA-end of the tRNA in the ribosomal A site (**Figure 4C, i** and **ii**), suggesting that these ribosomes are in the post-peptidyl transfer state, after the peptide bond formation, but before tRNA translocation. A majority of the ribosomes trapped in this state by Rbg1/Tma46 (~92% of the total ribosomal complexes found in this study) assume the classical ligand-binding state with both A- and P-tRNA bound (**Figure 4C, i**). In comparison, an earlier study showed that ~64% of translating ribosomes prepared in a similar manner are in the classical state [23]. This suggests that the Rbg1/Tma46 complex prefers to associate with ribosomes in the classical state. While these ribosomes are in the classical ligand binding state, a more detailed analysis shows that the head region of the 40S subunit and the P-tRNA have considerable conformational flexibility in the ribosome. By contrast, the conformation of the A-tRNA with an attached nascent peptide is more "fixed", with fewer degree of rotation (**Figure 4D**).

In addition to the classical ligand binding conformation, ~4.4% of the ribosomal complexes are in a rotated state, which contains A/P-site and P/E-site tRNAs (**Figure 4C, ii**).

The remainder of the ribosomal complexes carry the translational elongation factor 2 (eEF2) in the GAC but contain no tRNAs. They belong to translationally inactive "sleeping" ribosomes [25].

Although we employed focused classifications of the ribosomal P and E sites, as well as the A-site with the GTPase associated center (GAC), where a typical translational GTPase binds, we were not able to identify the Rbg1/Tma46 complex in the structure. This is likely due to conformational flexibility of the protein heterodimer, especially in the N-terminal region of Tma46 which contains its zinc finger motifs.

DISCUSSIONS

Rbg1/Tma46 complex alleviates ribosome pausing and helps promote efficient translation at R-/K-rich sequences

Despite their highly conserved nature, functions of Drg proteins and their regulatory partner Dfrps remain enigmatic. Here, using genomic, molecular and structural methods, we demonstrate molecular functions of the yeast Drg1/Dfrp1 orthologs, Rbg1/Tma46, in translation. In our genomic investigation, we observed initiation arrest and a decline of elongation rates on mRNAs in all mutant strains used in the study: Δrbg1, Δrbg2Δslh1 and Δrbg2Δslh1-Rbg1d. It is conceivable that the observed initiation arrest and elongation rate decline are coupled. *Remarkably, these negative impacts are accumulative, with the mildest defect occurring in the single knockout and the most severe defect occurring in the Δrbg2Δslh1-Rbg1d cell.* Subsequent analysis indicates ribosome pausing at R/K-rich sequences underlines the observed initiation and elongation defects. Translation of genes involved in ribonucleoprotein complex biogenesis and noncoding RNA processing pathways are most affected when Rbg1 protein is absent.

Our single-particle cryoEM reconstruction showed that the Rbg1/Tma46 complex targets translating ribosomes at the post-peptidyl transfer state, after peptide-bond formation but before EF2 binding and tRNA translocation. How does Rbg1/Tma46 alleviate ribosome pausing and help promote efficient translation at R-/K-rich sequences? Based on our structure, the ribosomal decoding and peptidyl transferase centers assume an unaltered, substrate-accommodating conformations when Rbg1/Tma46 binds, in contrast to the altered conformations reported when a polybasic peptide resides in the exit tunnel without this protein complex [26-28]. Furthermore, a majority (94%) of Rbg1/Tma46-bound ribosomes are in the classical ligand binding state. These observations strongly suggest that binding of Rbg1/Tma46 likely facilitates the peptide bond formation at the peptidyl transferase center when translating the R/K-rich sequences.

Nevertheless, since a small fraction of Rbg1/Tma46-enriched ribosomes (~4.4%) are in the hybrid ligand binding state, another possibility could be that Rbg1/Tma46 complex assists with tRNA movement in the ribosome. Of course, considering the roles of Slh1 [23,29-32], we cannot completely rule out the possibility that this protein complex participates in ribosome-assisted protein quality control pathways [33-36].

Similar to Slh1 [23], the site where the Rbg1/Tma46 complex binds in the ribosome remains unresolved. Results from our biochemical and EM studies using gold-labeled Rbg1 protein suggest that the complex mainly associates with the large ribosomal subunit in the vicinity of the E and P sites. Furthermore, the flexible RNA region of the L1 stalk and other flexible RNA regions on the surface of the ribosome are unlikely to be the direct binding locations, as indicated by the results obtained from our limited RNase I-treatment of the

ribosomal complex (**Supplemental Figure 6**). Exterior proteins or interior ribosomal regions, as well as ribosome-bound ligands, such as tRNAs, could conceivably be the targets. Our UV-crosslinking results show that Rbg1 crosslinks to a subset of tRNAs *in vivo* (Jin Lab, unpublished data) and the Rbg1/Tma46 complex directly binds to tRNAs with considerable affinity *in vitro* (**Supplemental Figure 8**). Obviously, further investigations are required to reveal these important interactions.

Possible functions of Drg1/Dfrp1, Drg2/Dfrp2 and ASCC3 (Rbg1/Tma46, Rbg2/Gir2 and Slh1 in yeast)

The accumulative effects observed in this study among Δrbg1, Δrbg2Δslh1, and Δrbg2Δslh1-Rbg1d strains strongly suggest overlapping functions for Drg/Dfrp and ASCC3 (the mammalian counterpart of Slh1) proteins in fundamental biological processes. While it is not entirely impossible that these protein complexes always target modules or subunits of the same complex in the cell, it is perhaps more reasonable to assume that the direct cellular targets and molecular functions of these proteins are different, as dictated by their different molecular nature including distinct sequences, structures, and characterized functions such as the catalytic hydrolysis of distinct NTPs among Rbg1/Tma46, Rbg2/Gir2, Slh1 and their mammalian counterparts. Despite this, the function of their different actions contributes to highly conserved pathways. Here, we propose this group of proteins functions by targeting different complexes involved at discrete stages of an essential pathway, whereby protein homeostasis is ensured in the cell. Based on our data and results published so far, protein synthesis and quality control pathways are their targets. Several lines of evidence support this hypothesis.

First, The reduced fitness of yeast cells as a result of double, but not single mutants of the Rbg protein family members (Rbg1, Rbg2, Tma46, and Gir2) [37] suggests a partially-overlapping functional consequence between the two Rbg complexes. Yeast genetic screens followed by biochemical investigations showed that one of either the Rbg1/Tma46 or Rbg2/Gir2 complexes was required for uncompromised growth of yeast cells lacking the slh1 gene [38]. The protein product of this gene, Slh1, is another highly conserved eukaryotic protein which associates with translating ribosomes [13] and functions in the ribosome-associated quality control (RQC) and No-go decay (NGD) pathways [23,29-32]. Simultaneous functional inactivation of Rbg1, Rbg2, and Slh1 results in detrimental effects to the cell.

Second, our data demonstrate that the Rbg1/Tma46 complex alleviates ribosome pausing on R/K-rich sequences at the post-peptidyl transfer state in translation. Due to the conserved nature of this complex, a similar function is likely to be observed in higher eukaryotic organisms. Thus, it is conceivable that the Drg1/Dfrp1 complex directly targets to the translation pool via association with the translation apparatus for the protein quality control.

In contrast, the Drg2/Dfrp2 complex likely targets to the non-translation pool for a similar purpose. All of the Drg2/Dfrp2 complexes identified so far associate with the non-polysomal fraction when assayed using sucrose-gradient fractionation methods. Furthermore, Drg2/Dfrp2 remain associated with non-polysomal fractions in HEK293 cells when the drg1 gene is deleted (Jin Lab, unpublished data). These observations suggest that Rbg2/Gir2 is likely acting on the non-translation pool to ensure protein homeostasis in the cell. How could this complex help a paused translational apparatus in such an indirect way? One possibility is that it could titrate out proteins that physically remain in the translation pool but functionally

undermine the same quality control process. Another possible function is to alter the equilibrium and/or kinetics of steps of a reaction involved in the same pathway. Obviously, further investigations are required to provide details at the molecular level.

Furthermore, the weak cross-association of Drg1 and Dfrp2, but not Drg1 and Dfrp1 (--No Drg2 and Dfrp1 association was observed so far), in the otherwise specific and distinct complexes, rules out the strict exclusiveness of the two Drg/Dfrp classes and suggests another fine-tuned layer of control in the cell.

Drg proteins play important roles in some cellular processes seemingly unrelated to translation. For example, they are involved in spindle checkpoint signaling, also elevated levels of Drg1 protein causes lung adenocarcinoma and taxol resistance [39]. In an *in vitro* study, Drg1 was reported to diffuse on microtubules, to promote microtubule polymerization, and to drive microtubule bundle formation in a GTP-independent manner [40]. HeLa cells with reduced Drg1 levels show delayed progression from prophase to anaphase due to a slowed spindle formation [40]. Further investigations are required to see if these seemingly unrelated processes link with translation.

Maintaining protein homeostasis during critical stages and conditions such as development, proliferation, and cellular stress conditions is critical for eukaryotic organisms. It is not surprising that the translational machinery is one of the major targets of regulation for this purpose. Our observations provide links between translation pausing and protein quality control, a critical component in maintaining protein homeostasis and cell physiology. It is worth mentioning that other pathways may crosstalk with these processes to achieve the same goal.

A

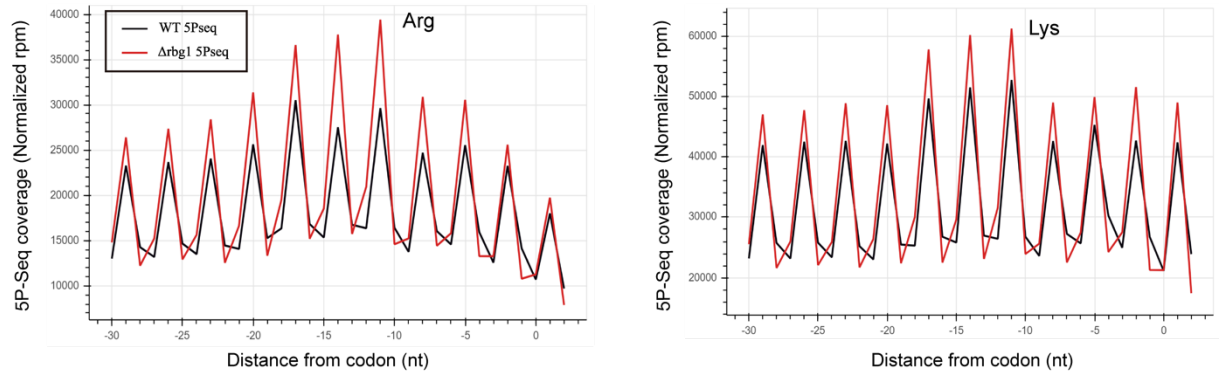

B

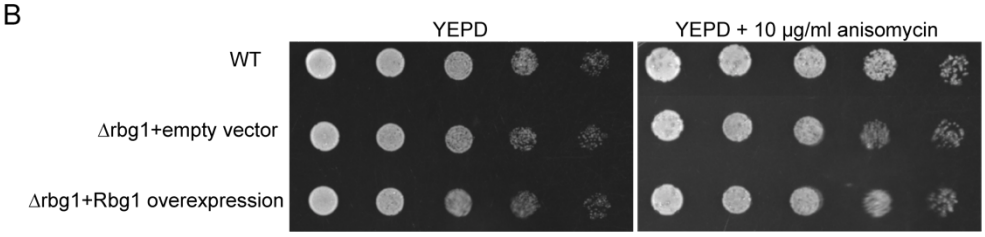

C

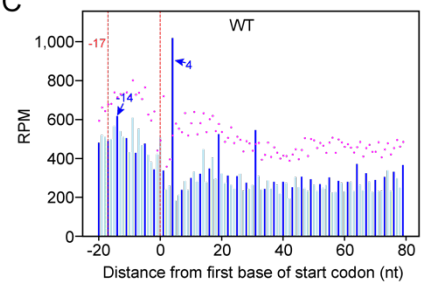

D

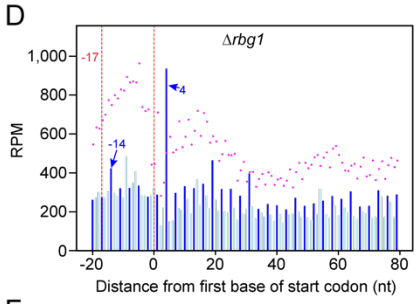

E

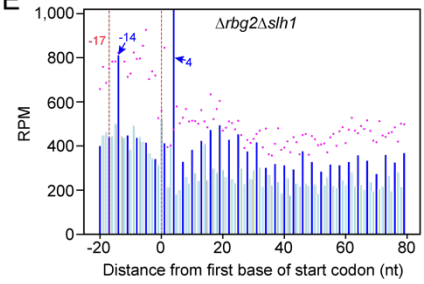

F

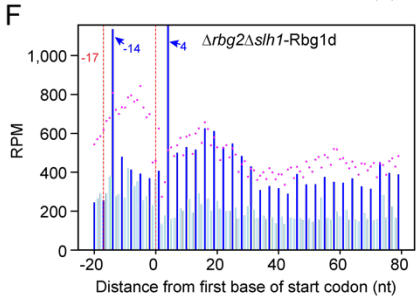

G

Gene Ontology Term	Count	FDR
ribonucleoprotein complex biogenesis	79	2.1E-12
ribosome biogenesis	68	1.7E-11
rRNA metabolic process	49	3.9E-7
rRNA processing	47	5.6E-7
cellular component biogenesis	123	3.5E-6
ncRNA metabolic process	63	1.5E-4
ribosomal small subunit biogenesis	27	6.7E-4
ncRNA processing	51	1.0E-3
ribosomal large subunit biogenesis	24	1.4E-3
ribonucleoprotein complex assembly	31	2.0E-3

Figure 1. Translation initiation arrests in mutant strains.

A. **Increased ribosome pausing when translating Arg and Lys in the absence of Rbg1**. The metagene (-30 to +10 window) which shows the number of 5P intermediates for Arg and Lys amino acids and their positions. The total number of reads was normalized to facilitate data analysis and comparison. The -17nt, -14nt and -11nt peaks represent indicated codons at the ribosomal A, P and E sites, respectively.

B. Deletion of Rbg1 results in slower growth for yeast cells in the presence of anisomycin. Expression of Rbg1 protein in the Δrbg1 cells restored growth. Δrbg1 cells were transformed with either an empty vector, or a vector containing the rbg1 gene with a PGK1 promoter. Serial dilutions of exponential phase liquid cultures were spotted on YEPD, with or without 10 µg/ml anisomycin, and were incubated at 30 ˚C for 2 days.

C-F: Normal pausing at start codons in wild type cells (C). Increased ribosome pausing at start codons in Δrbg1 (D), Δrbg2Δslh1 (E), and Δrbg1Δslh1-Rbg1d (F) strains. Metagene analysis displaying the abundance of 5'P reads relative to start codons for WT (C), Δ*rbg1* (D), Δ*rbg2*Δ*slh1* (E), and Δ*rbg2*Δ*slh1*-Rbg1d (F) strains, or after random fragmentation (5PSeq control, dotted magenta line). Reads are represented by RPM, with the blue bar indicating the +1 frame and light blue bars indicating the 0 and +2 frames. The two dotted red lines show the positions of 0 and -17 nt relative to the start codon. The blue peak at -14 nt corresponds to the protected region from a putative initiation-paused ribosome and the peak at 4 nt is caused by peptide induced ribosomal arrest. Biological replicates are averaged.

G: Gene ontology analysis suggests that the genes which show ribosome pausing at the initiation site in the Δrbg2Δslh1-Rbg1d strain are related to ribonucleoprotein complex biogenesis and ncRNA processing pathways. By filtering the ratio of reads at -14 nt to the surrounding ± 2 codons larger than 0.1, 353 genes were selected from the Δ*rbg2*Δ*slh1*-Rbg1d strain for Gene ontology analysis using DAVID [41]. The top 10 gene ontology terms for biological processes were shown, ranked by false discovery rate (FDR).

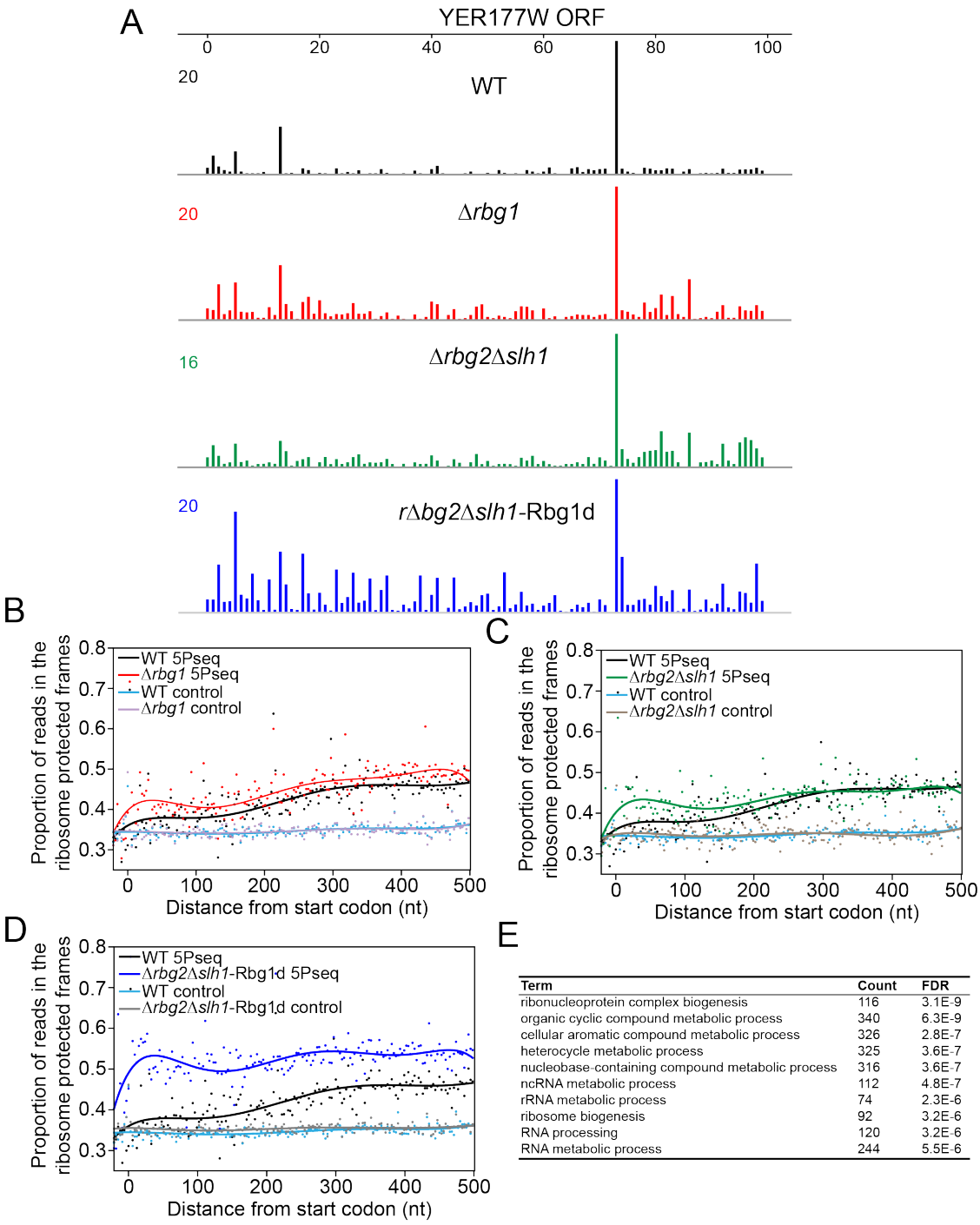

Term	Count	FDR
ribonucleoprotein complex biogenesis	116	3.1E-9
organic cyclic compound metabolic process	340	6.3E-9
cellular aromatic compound metabolic process	326	2.8E-7
heterocycle metabolic process	325	3.6E-7
nucleobase-containing compound metabolic process	316	3.6E-7
ncRNA metabolic process	112	4.8E-7
rRNA metabolic process	74	2.3E-6
ribosome biogenesis	92	3.2E-6
RNA processing	120	3.2E-6
RNA metabolic process	244	5.5E-6

Figure 2: Slower translational elongation after depletion of Rbg1, Rbg2, and Slh1.

A. Representative genome tracks of the 5' ends of 5PSeq reads in WT (black), Δ*rbg1* (red), Δ*rbg2*Δ*slh1* (green), and Δ*rbg2*Δ*slh1*-Rbg1d strains (blue). Coverage is expressed in RPM. An obvious 3-nt periodicity pattern was observed for YER177W mRNA in the Δrbg2Δslh1-Rbg1d strain.

B-D: The proportion of 5PSeq reads in the ribosome-protected frame (Frame 1 in **Supplementary Figure 2**) shows that the 5' end of mRNA was protected by ribosomes in the Δrbg2Δslh1-Rbg1d strain. Proportion scores were calculated for each codon by normalizing the read counts in frame 1 to the total reads in all three

frames within the same codon. These are shown as dots with smoothed lines (polynomial fitting) for genes longer than 1000 base pairs (bp) and with RPKM values > 20. Only the region containing -20 nt to 501 nt with respect to the first base of start codon were used to calculate the proportion score. 5Pseq samples from Δ*rbg1* (B, red), Δ*rbg2*Δ*slh1* (C, green), and Δ*rbg2*Δ*slh1*-Rbg1d (D, blue) strains were compared to WT strains (black). Random fragmentation samples (control) are also shown. Biological replicates are averaged.

E: Gene ontology analysis of the 715 genes which have higher proportion scores in the Δ*rbg2*Δ*slh1*-Rbg1d strain, when compared to WT strain, show that the genes which have slower elongation rates in the Δrbg2Δslh1-Rbg1d strain are related to the ribosome biogenesis and ncRNA processing pathways. The range of -12 nt to 99 nt, with respect to the first base of start codon, was used to calculate the proportion score. Genes whose proportion scores were larger than 0.4 in the Δ*rbg2*Δ*slh1*-Rbg1d strain, and whose proportion scores were more than 1.5 times the scores found in the WT strain were selected and analyzed by DAVID [41]. The top 10 GO terms for biological processes are shown, ranked by false discovery rate (FDR).

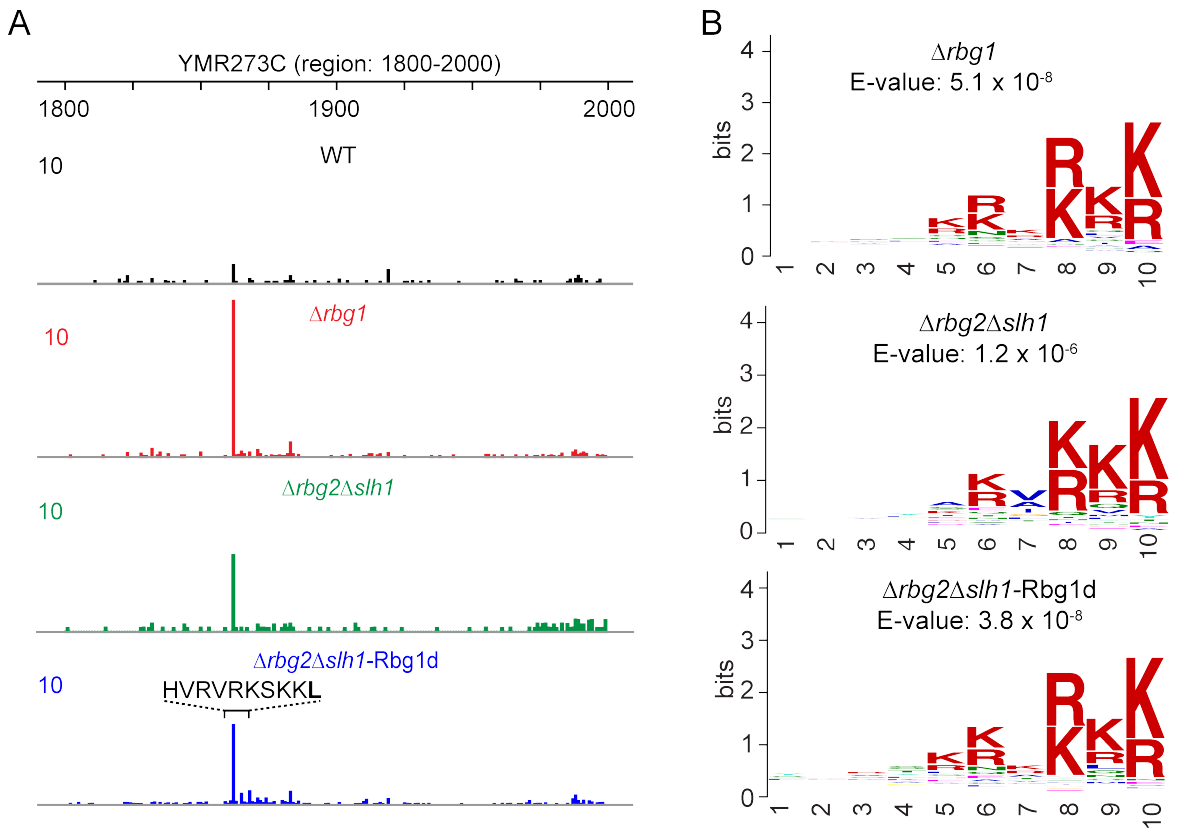

Figure 3. Rbg1 alleviates ribosome pausing at arginine/lysine-rich regions.

A. Representative genome tracks of 5' ends of 5PSeq reads. Genome tracks of the 5' ends of 5PSeq reads in WT (black), Δ*rbg1* (red), Δ*rbg2*Δ*slh1* (green), and Δ*rbg2*Δ*slh1*-Rbg1d (blue) strains were shown around the arginine-/lysine-rich region. Coverage is expressed in average RPM of the biological duplicates.

B. Translation pauses at the R-/K-rich region in Δ*rbg1*, Δ*rbg2*Δ*slh1*, and Δ*rbg2*Δ*slh1*-Rbg1d strains. To identify specific peptide sequences which induce ribosome pausing while being translated in the knockout strains, pause scores were first calculated by dividing the RPM value at each position of the transcript by the mean RPM value for the ten codons upstream and downstream of the same position. The ten amino acids upstream with a pause score > 10 were compared to those with pause scores < 10 using MEME [42]. Amino acid sequences extracted from the WT strain show no consensus sequence.

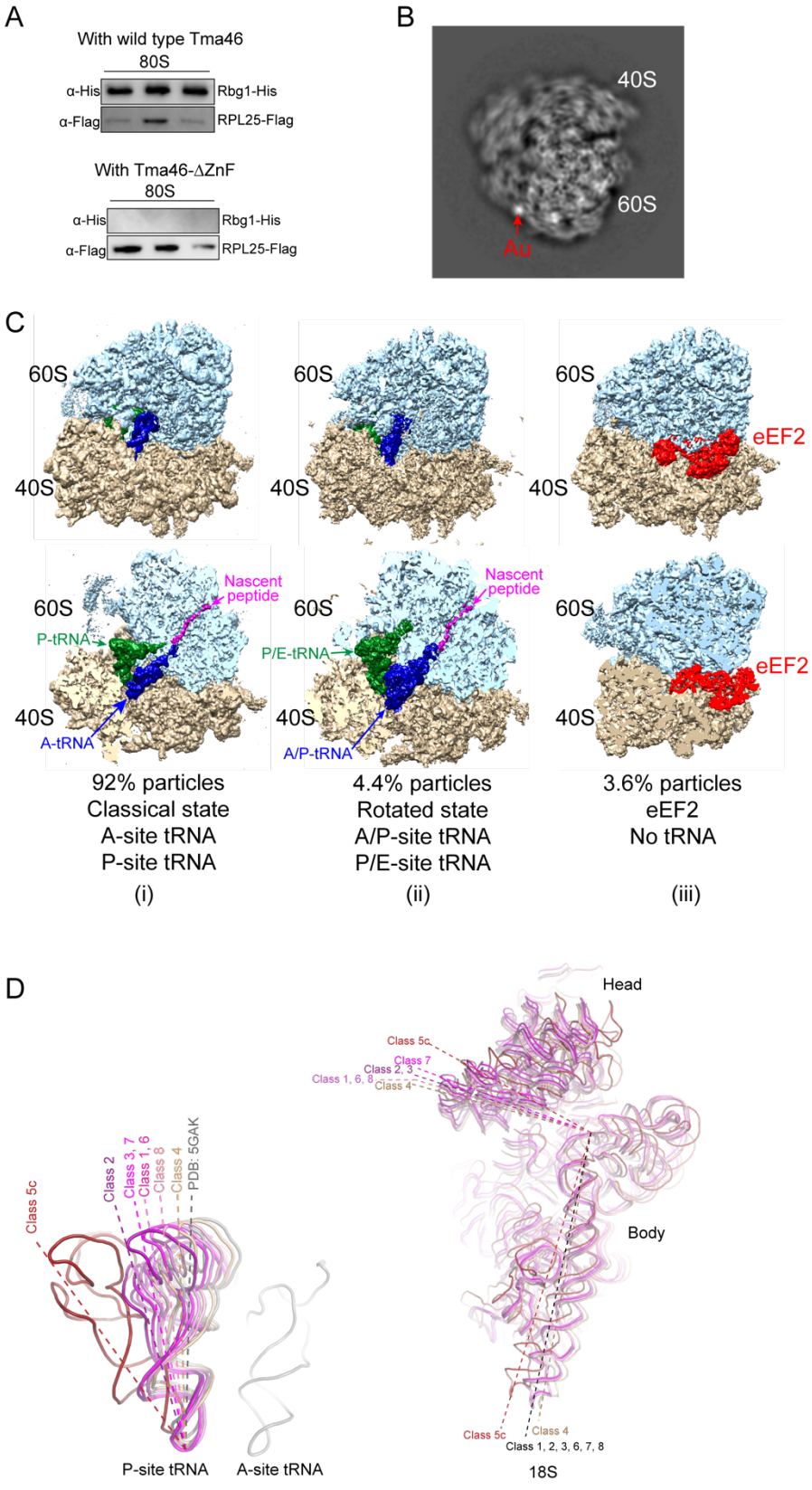

Figure 4: Rbg1/Tma46 complex associates with the large ribosomal subunit via the zinc-finger domain of Tma46 and targets translating ribosomes in the post-peptidyl transfer state.

A. **The Rbg1/Tma46 complex binds to the ribosome via the zinc-finger domain of Tma46**. Proteins co-expressed in the *E.coli* BL21 strain were purified and incubated with pure 80S ribosomes, then ribosomal complexes were separated by sedimentation through a 10-50% sucrose gradient. Binding of Rbg1/Tma46 to the ribosome was determined by western blot. Flag-tagged RPL25 was immunoblotted on the same membrane

B. **2D classification analysis for gold-labelled samples**. Rbg1-associated ribosomes were purified from micrococcal nuclease-treated cell extracts, where Rbg1 was endogenously tagged with a 6xHis epitope. Purified complexes were incubated with gold-NTA particles, and unbound gold was removed by gel filtration. CryoEM micrographs were collected and 2D classification was performed on these gold-labelled samples. The bright spots, indicated by red arrows, are the gold particles associated with the complex.

C. **CryoEM analysis of Rbg1/Tma46-bound ribosomes.** Rbg1/Tma46-bound ribosomes from the whole-cell extract were obtained via affinity pulldown of C-terminally Flag-tagged Rbg1 in the polysome fraction. CryoEM was directly performed, and 6,725 micrographs were collected. After 2D and 3D classification, 209,143 ribosomal particles were further analyzed by focused classification using Relion. Of these ribosomal particles, 92% (192,134) are ribosomes in the classical ligand-binding state, containing A- and P-site tRNA (i); 4.4% (9,293) are in a rotated state, with A/P- and P/E-site tRNA bound (ii); and the remaining 3.6% (7,716) of ribosomes are only bound with eEF2 (iii). The top panel shows the global map of ribosomal complexes and the bottom panel contains the "clipping map" showing ligands buried inside of the ribosomes. 60S subunits are colored in light blue and 40S subunits are shown in yellow. P-tRNAs (or P/E-tRNAs), A-tRNAs (or A/P-tRNAs), nascent peptides, and eEF2 ligands are colored in green, blue, magenta, and red, respectively.

D. Rotations of P-tRNAs and 40S subunits in the Rbg1/Tma46 bound ribosomes.
Left panel: Conformational flexibility of P-tRNAs. A- and P-tRNAs are fitted into the density of the obtained cryoEM maps using rigid-body fitting. In all classes obtained, the A-tRNA conformations are very similar except for those in the Class 5c, which contains hybrid A/P-tRNA (red backbone). P-tRNAs, on the other hand, demonstrate various degrees of rotation/displacement towards the ribosomal E-site. A- and P-tRNAs bound to ribosome in the classical state, with eIF5A bound to the E-site (PDB code: 5GAK) are shown in gray as a reference. **Right panel: Conformational flexibility of 40S:** Diagrams of the 18S rRNA. The body, head, and shoulder domains of 40S and 60S subunits were rigid-body fitted into the maps individually. 40S subunits from different classes show different rotation angles when the 60S subunits were aligned. Ribosomal proteins were not shown.

METHODS

Yeast strains, plasmid constructs and growth conditions

Saccharomyces cerevisiae strains with BY4742 (*MATα his3Δ1 leu2Δ0 lys2Δ0 ura3Δ0*) background were used in this study. Chromosomal insertion and knockout strains with this background were obtained by established homologous recombination techniques [43,44], and are listed in **Supplemental Table 1**. The plasmids used here were constructed via standard cloning strategies and are listed in **Supplemental Table 2**. To generate C-terminal, chromosomally Flag-tagged strains, the TEV-6xHis-3xFlag-*URA3* cassette, contained in the modified p415G plasmid, was amplified with homology regions to replace the stop codon of the gene to be tagged. Strains were confirmed by sequencing across the entire fusion gene, as well as western blot detection of the Flag epitope. It has been reported that cellular growth of the *rbg1*Δ*rbg2*Δ*slh1*Δ strain was severely impaired [13]. To control the Rbg1 protein level in the cell, a mini auxin-inducible degron (mAID) tag was inserted chromosomally into the *rbg2*Δ*slh1*Δ strain, at the 5' end of the Rbg1 gene, with a sequence containing the *KanMX*-GAL10p-mAID-Flag epitope before the start codon of Rbg1 [21].

Genes encoding Rbg1 and Tma46 were amplified from the genomic DNA of *S. cerevisiae* and were cloned into modified pET28a or pET22b vectors using standard cloning strategies. Mutants were generated by mutagenesis PCR using the Q5 Site-Directed Mutagenesis Kit (NEB), according to the manufacturer's instructions.

To obtain polysome profiles and perform 5Pseq experiments, wild type and mutant cells were grown to an OD_{600} of 0.6 in YPGR (2% galactose + 0.2% raffinose) medium at 30 ˚C, harvested by centrifugation, then washed and resuspended in the same volume of YEPD (2% glucose) medium containing 1 mM auxin (Sigma). These cells were grown in the presence of auxin for another 20 minutes at 30 ˚C to deplete Rbg1 completely.

Purification of ribosomes, tRNAs and proteins

Yeast ribosomes from the YAS2488 strain were purified according to published methods (Acker et al., 2007 and Fernandez et al., 2013). Yeast $tRNA_i^{Met}$ and $tRNA^{Phe}$ were prepared by *in vitro* transcription [45,46]. Wild type and mutant Rbg1 and Tma46 were cloned and overexpressed in BL21(DE3) cells, then purified by affinity and ion-exchange chromatography [7].

Filter binding assay

The binding constants of tRNA with purified Rbg1 and Tma46 were measured using a filter binding assay as described [47] with minor modifications. ^{32}P-labeled tRNA [48,49] was incubated with the Rbg1/Tma46 complex in binding buffer (25 mM HEPES-KOH, pH 7.6, 2.5

mM $Mg(OAc)_2$, 80 mM KOAc, 2 mM DTT, 0.5 mM GDPCP•Mg^{2+}) at 30 ˚C for 10 minutes. The reaction solution was subsequently filtered through two membranes simultaneously, the first being a nitrocellulose membrane (GE Healthcare Amersham) and the second being a Nytran Supercharge membrane (Whatman). The [^{32}P]-tRNA bound to Rbg1/Tma46 is retained on the nitrocellulose filter and free [^{32}P]-tRNA passes through the nitrocellulose filter and is retained on the Nytran Supercharge membrane. The bound and unbound [^{32}P]-tRNA were quantified by scintillation counting.

Cell growth assay

Cell growth rates were determined by a spot assay as reported [50] with minor modifications. Cells were first grown to exponential phase at 30 ˚C in either YPGR or YEPD, depending upon the strain used. Then 0.5 OD_{600} units of cells were pelleted down and resuspended in 0.5 ml of 1X PBS buffer. The following serial dilutions were prepared in 1 x PBS buffer: 1/5, 1/25, 1/125, and 1/625, and 1 µl of each dilution was spotted on YEPD agar plates. 1 mM auxin (Sigma) was added for assays of Δrbg1Δslh1-Rbg1d strains. Images were taken after 2 to 5 days of growth at 30 ˚C.

Polysome profiling

Yeast cells were grown at 30 ˚C until they reached an OD_{600} of 0.6, then were treated with 100 µg/ml of cycloheximide for 2 minutes before harvesting. Cells were quickly harvested by centrifugation and were washed twice with ice-cold polysome lysis buffer (20 mM Tris-HCl, pH 8.0, 140 mM KCl, 1.5 mM $MgCl_2$, 1% (v/v) Triton X-100, 1 mM DTT, 100 µg/ml cycloheximide). The cell pellet was resuspended in 1 ml of polysome lysis buffer supplemented with EDTA-free protease inhibitors (Roche) and was grounded in liquid nitrogen using an RNase-free mortar and pestle. Extracts were clarified at 18,000 × *g* for 10 minutes at 4 ˚C, then loaded onto 10%-50% sucrose gradients in polysome gradient buffer (20 mM Tris-HCl, pH 8.0, 140 mM KCl, 5 mM $MgCl_2$, 20 U/ml SUPERase.In, 0.5 mM DTT, 100 µg/ml cycloheximide). Gradients were centrifuged at 32,000 rpm for 3 hours and 45 minutes in a Beckman SW 32.1 Ti rotor and polysome profiles were generated by fractionation with continuous measurement of absorbance at 260 nm. Equal volumes of the fractions were collected, and proteins of interest were analyzed by western blot. For RNase treatments, 15 Units of RNase I were added per 1 OD_{260} of cell extract, then the reaction mixture was incubated for 2 hours at 23˚C.

Western blot

Western blotting was performed as described [46]. Fractions from polysome profiles were resolved via SDS-PAGE, and proteins of interest were transferred to nitrocellulose membranes (GE Healthcare Amersham) for 40 minutes at 100 V in a Mini Trans-Blot apparatus (Bio-Rad).

Protein bands were detected with either anti-Flag (Sigma-Aldrich) or anti-His antibodies (Sigma-Aldrich).

5Pseq library preparation

5Pseq libraries were prepared as described [18,51]. Yeast strains were grown in 50 ml YPGR medium until they reached an OD_{600} of 0.6. Cells were then harvested and their media exchanged for 50 ml YEPD containing 1 mM auxin (Sigma), followed by an additional 20 minutes of incubation. Cells were harvested quickly by centrifugation. Total RNA was extracted and DNA was removed by incubation with TURBO DNase (Ambion) for 30 minutes at 37 ˚C. For control libraries, 50 µg of DNA-free total RNA was fragmented by incubation at 80 ˚C for 5 minutes in RNA fragmentation buffer (40 mM Tris-acetate, pH 8.1, 100 mM KOAc, 30 mM $Mg(OAc)_2$). Fragmented 5'-OH sites were phosphorylated by treatment with 5 units of T4 polynucleotide kinase (NEB) for 1 hour at 37 ˚C, followed by phenol:chloroform extraction. The phosphorylated 5'-ends were subjected to RNA ligation by 20 units of T4 RNA ligase 1 (NEB) in the presence of 10 mM DNA/RNA rP5_RND oligo (**Supplemental Table 3**) at 16 ˚C overnight. For the 5Pseq libraries, 50 µg of DNA-free total RNA was directly ligated to the rP5_RND oligo in the same conditions as specified for control samples. The polyadenylated mRNAs were enriched using Dynabeads $(dT)_{25}$ (Life Technologies), according to the manufacturer's instructions, followed by fragmentation for 5 minutes at 80˚C in RNA fragmentation buffer. Both the controls and 5' RNA-seq samples were primed with random hexamers and reverse transcribed with Superscript II (Life Technologies). Second strand cDNA synthesis was performed using a single PCR cycle (98 ˚C for 1 minute, 50 ˚C for 2 minutes, and 72 ˚C for 15 minutes) in Phusion High-Fidelity PCR Master Mix and was primed with BioNotI-P5-PET (**Supplemental Table 3**). Double-stranded cDNA was purified using HighPrep beads (Magbio), then was bound to Dynabeads M-280 Streptavidin beads (Life Technologies). Bound DNA molecules were subjected to end repair, adenine addition, and adaptor ligation via addition of 0.5 µL of P7MPX annealed adaptor, which was prepared by annealing the P7MPX_linker_for and P7MPX_linker_rev (**Supplemental Table 3**) primers at a final concentration of 2.5 µM. The Dynabead-bound DNA was washed and subjected to PCR amplification (98 ˚C for 30 seconds; 18 cycles of the following condition: 98 ˚C for 20 seconds, 65 ˚C for 30 seconds, 72 ˚C for 30 seconds; 72 ˚C for 5 minutes) using Phusion High-Fidelity PCR Master Mix with HF buffer (NEB), 0.1 µM of PE1.0, and the appropriate PE2_MPX_01 to PE2_MPX_08 primers (**Supplemental Table 3**). Samples were size-selected using 0.6x-0.9x (v/v) HighPrep beads (Magbio), separated via agarose gel electrophoresis, and the 300-500 bp regions of the gel were extracted. Libraries were sequenced using single-end, 100bp-read NovaSeq Illumina sequencing with 6 nt indexing reads for library identification.

High throughput sequencing data processing and analysis

For all libraries, reads were first demultiplexed using the index sequences. The 3' adaptor sequence was identified and removed using the cutadapt package [52]. After adaptor removal, the remaining reads were deduplicated by bbmap (BBMap - Bushnell B. -

sourceforge.net/projects/bbmap/) based upon random barcode sequences, and the 5' UMI were trimmed by fastx_trimmer (Hannon, G.J. (2010) FASTX-Toolkit.). Non-coding RNAs were filtered by mapping to annotated *S. cerevisiae* rRNAs, tRNAs, snRNAs, and snoRNAs using Bowtie1 [53]. Unaligned reads were then mapped to the sacCer3 genome using Bowtie2 [54] with the arguments: '--local -D 15 -R 2 -N 1 -L 20 -i S,1,0.75 -S'.

Unless indicated otherwise, data analysis was performed using a series of custom scripts written in Python. For 5Pseq experiment, reads with multiple alignments, mapping quality values < 30, or those containing soft-clipped bases on the 5' end were excluded from downstream analysis. The 5' ends of reads passing quality filtering were extracted and the total numbers of reads per genome location were calculated. Reads per million (RPM) values for each genomic locus were calculated using the number of unique reads. Only genes with reads per million per kilobase (RPKM) values of greater than 20 were chosen for further analysis. To create meta gene plots, we calculated the average rpm of the 5' ends from all biological replicates. These 5' ends were then aligned relative to the stop codon (or any specific codon) of all ORFs, and the sum of the 5' ends reads was determined at each position. To analyze ribosome pausing around the start codon, genes were sorted by a ratio value which is calculated by dividing the read counts at -14 nt or 4 nt by the total read counts corresponding to the surrounding ±2 codons, as previously described [18]. Then the first 8 amino acids of the ORF were extracted. Sequences of the top 50% of genes were compared to the bottom 50% using MEME [42]. To characterize the elongation pausing, we calculated the pause score, as described previously, with minor modifications [22]. Pause scores were calculated by dividing the rpm value at each genomic position by the mean of the rpm values in the ±10-codon region surrounding the position. Regions in the first and last 10 codons of the ORF were excluded. Amino acid sequences with pause scores > 10 were considered to be stalling sites. Stalling sequences were calculated by MEME [42] using the sequences with pause score <10 as a control.

Electron microscopy, data collection and image processing

Saccharomyces cerevisiae with C-terminally His/Flag-tagged Rbg1 were grown to log phase at 30 ˚C, then were treated with 0.1 mg/ml of cycloheximide for 2 minutes before being harvested by centrifugation. The harvested cells were resuspended in polysome lysis buffer and frozen in liquid nitrogen.

For direct pulldowns of Rbg1/Tma46-bound ribosomal complexes, cell extracts were incubated with anti-Flag resin overnight at 4˚C. The complex-bound resin was washed three times with polysome lysis buffer, and the Rbg1/Tma46 bound ribosomal complexes were eluted with 3xFlag peptide.

For the RNase-treated samples, 15 Units of RNase I were added per 1 OD_{260} of cell extract and incubated for 2 hours at 23˚C. The 80S complexes were purified using a 10-50%

sucrose gradient, followed by incubation with anti-Flag resin for 3 hours at 4 ˚C and a subsequent elution with 3xFlag peptide.

For gold-labeled ribosomal complex samples, cell extracts were incubated with 0.8 mM $CaCl_2$ and 1 Unit/OD_{260} of S7 micrococcal nuclease (Roche) for 20 min at room temperature to obtain a monosomal solution. This reaction was stopped by the addition of 2 mM ethylene glycol tetraacetic acid, then was loaded onto a 10%-50% sucrose gradient in polysome gradient buffer for centrifugation at 32,000 rpm in a Beckman SW32.1 rotor for 3 hours 45 minutes. The monosomal fraction was collected and incubated with anti-Flag resin for 3 hours at 4˚C. This sample was washed with lysis buffer three times before elution with 3xFlag peptide. The eluted ribosomal complexes were incubated with a 10-fold excess of 1.8 nm Ni-NTA-Nanogold (Nanoprobes). Unbound Ni-NTA-Nanogolds were removed by gel filtration.

Sample preparation for cryoEM studies was performed as described [55]. 2.5 µl aliquots of gold-labeled ribosomal complexes were incubated for 30 seconds on glow-discharged Holley carbon grids with a thin-layer carbon film cover (Quantifoil). Grids were blotted using a Vitrobot Mark IV (FEI) for 2.5 seconds in 100% humidity at 4 ˚C, then were plunge frozen into liquid ethane. Data for native pullouts and RNase-treated samples were collected in vitreous ice using Titan Krios and JEOL 3200FS transmission electron microscopes, both operating at 300 keV. Microscopes used were equipped with K2 summit direct electron detectors (Gatan). 6,725 micrographs were acquired for the native sample, and 520 micrographs were acquired for the RNase-treated sample. Data for gold-labeled samples were collected in vitreous ice using a Titan Krios electron microscope operating at 300 keV, equipped with a K3 summit direct electron detector (Gatan). 933 micrographs were acquired. The drifts of movie frames were corrected using MotionCor2 [56], and the contrast transfer functions were determined using CTFFIND4 [57].

Data processing was carried out in Relion3 [58]. Rigid-body fitting was performed in Chimera [59]. Figures were made in Chimera [59] and Pymol [60]. Resolutions were reported based upon the gold-standard Fourier shell correlation (FSC) of 0.143 criterion [61].

For the sample prepared by direct affinity-pulldown of Rbg1 from the cell 706,323 particles were automatically picked in Relion software using Laplacian-of-Gaussian, extracted, and subjected to reference-free 2D classifications to remove non-ribosomal particles. 3D classification was employed to remove the ribosomal subunits. 209,143 good ribosomal particles were selected for final 3D classification (8 classes) using a mask including the A-, P- and E-site of the ribosome. Class 5 was further analyzed using focused classification with signal subtraction (FCwSS). 40S head, body and shoulder domains, as well as bound tRNAs were rigid-body fitted individually into the electron density maps obtained.

For the RNase-treated sample, 38,263 particles were selected automatically, extracted, and subjected to reference-free 2D and 3D classification. 21,165 particles were shown in the classical state with A- and P-tRNA in the ribosome.

For the gold-labeled ribosomes, five 2D image references were first calculated from the particles picked manually from the micrographs, then a full set of particles were automatically picked based on these 2D references. Reference-free 2D classification was applied to analyze the position of the gold signal.

Data availability

The sequencing data for 5P-seq experiment have been deposited in NCBI's Gene Expression Omnibus and are accessible through GEO series accession numbers GSExxx, GSExxx and GSExxx. Electron microscopy maps have been deposited in the Electron Microscopy Data Bank under accession codes EMD-xxxx … for the 7 classes in classical state from the native samples, EMD-xxx for eEF2 bound ribosomes, EMD-xxx for A- and P-tRNA and P- and E-tRNA bound ribosomes, EMD-xxx for RNase-treated ribosomes.

Acknowledgments

We thank National Center for CryoEM Access and Training (NCCAT) and Northwestern University for cryoEM data collection, Roy J. Carver Biotechnology Center at the University of Illinois at Urbana-Champaign for sequencing and members in the H. Jin laboratory for helpful discussions. H.J. acknowledges support from the National Institute of General Medical Sciences of the NIH (R01-GM120552).

All authors declare no conflict of interests

References Cited

1. Kumar, S., Tomooka, Y. & Noda, M. Identification of a set of genes with developmentally down-regulated expression in the mouse brain. *Biochem Biophys Res Commun* **185**, 1155-61 (1992).
2. Sazuka, T. et al. Expression of DRG during murine embryonic development. *Biochem Biophys Res Commun* **189**, 371-7 (1992).
3. Leipe, D.D., Wolf, Y.I., Koonin, E.V. & Aravind, L. Classification and evolution of P-loop GTPases and related ATPases. *J Mol Biol* **317**, 41-72 (2002).
4. Li, B. & Trueb, B. DRG represents a family of two closely related GTP-binding proteins. *Biochim Biophys Acta* **1491**, 196-204 (2000).
5. Ishikawa, K. et al. Cloning and characterization of Xenopus laevis drg2, a member of the developmentally regulated GTP-binding protein subfamily. *Gene* **322**, 105-12 (2003).

6. Ishikawa, K., Azuma, S., Ikawa, S., Semba, K. & Inoue, J. Identification of DRG family regulatory proteins (DFRPs): specific regulation of DRG1 and DRG2. *Genes Cells* **10**, 139-50 (2005).
7. Francis, S.M., Gas, M.E., Daugeron, M.C., Bravo, J. & Seraphin, B. Rbg1-Tma46 dimer structure reveals new functional domains and their role in polysome recruitment. *Nucleic Acids Res* **40**, 11100-14 (2012).
8. O'Connell, A., Robin, G., Kobe, B. & Botella, J.R. Biochemical characterization of Arabidopsis developmentally regulated G-proteins (DRGs). *Protein Expr Purif* **67**, 88-95 (2009).
9. Song, H. et al. Overexpression of DRG2 Increases G2/M Phase Cells and Decreases Sensitivity to Nocodazole-Induced Apoptosis. *The Journal of Biochemistry* **135**, 331-335 (2004).
10. Mahajan, M.A., Park, S.T. & Sun, X.H. Association of a novel GTP binding protein, DRG, with TAL oncogenic proteins. *Oncogene* **12**, 2343-50 (1996).
11. Zhao, X.-F. & Aplan, P.D. SCL binds the human homologue of DRG in vivo1The DRG cDNA sequence has been deposited in GenBank under accession number AF078103.1. *Biochimica et Biophysica Acta (BBA) - Molecular Cell Research* **1448**, 109-114 (1998).
12. Schenker, T., Lach, C., Kessler, B., Calderara, S. & Trueb, B. A novel GTP-binding protein which is selectively repressed in SV40 transformed fibroblasts. *J Biol Chem* **269**, 25447-53 (1994).
13. Daugeron, M.C., Prouteau, M., Lacroute, F. & Seraphin, B. The highly conserved eukaryotic DRG factors are required for efficient translation in a manner redundant with the putative RNA helicase Slh1. *Nucleic Acids Res* **39**, 2221-33 (2011).
14. Fleischer, T.C., Weaver, C.M., McAfee, K.J., Jennings, J.L. & Link, A.J. Systematic identification and functional screens of uncharacterized proteins associated with eukaryotic ribosomal complexes. *Genes Dev* **20**, 1294-307 (2006).
15. Ishikawa, K., Akiyama, T., Ito, K., Semba, K. & Inoue, J. Independent stabilizations of polysomal Drg1/Dfrp1 complex and non-polysomal Drg2/Dfrp2 complex in mammalian cells. *Biochem Biophys Res Commun* **390**, 552-6 (2009).
16. Ishikawa, K., Ito, K., Inoue, J. & Semba, K. Cell growth control by stable Rbg2/Gir2 complex formation under amino acid starvation. *Genes Cells* **18**, 859-72 (2013).
17. Wout, P.K., Sattlegger, E., Sullivan, S.M. & Maddock, J.R. Saccharomyces cerevisiae Rbg1 protein and its binding partner Gir2 interact on Polyribosomes with Gcn1. *Eukaryot Cell* **8**, 1061-71 (2009).
18. Pelechano, V., Wei, W. & Steinmetz, L.M. Widespread Co-translational RNA Decay Reveals Ribosome Dynamics. *Cell* **161**, 1400-12 (2015).
19. Grollman, A.P. Inhibitors of protein biosynthesis. II. Mode of action of anisomycin. *J Biol Chem* **242**, 3226-33 (1967).
20. Nishimura, K. & Kanemaki, M.T. Rapid Depletion of Budding Yeast Proteins via the Fusion of an Auxin-Inducible Degron (AID). *Curr Protoc Cell Biol* **64**, 20 9 1-16 (2014).
21. Schuller, A.P., Wu, C.C., Dever, T.E., Buskirk, A.R. & Green, R. eIF5A Functions Globally in Translation Elongation and Termination. *Mol Cell* **66**, 194-205 e5 (2017).
22. Guydosh, N.R. & Green, R. Dom34 rescues ribosomes in 3' untranslated regions. *Cell* **156**, 950-62 (2014).

23. Matsuo, Y. et al. Ubiquitination of stalled ribosome triggers ribosome-associated quality control. *Nat Commun* **8**, 159 (2017).
24. Letzring, D.P., Wolf, A.S., Brule, C.E. & Grayhack, E.J. Translation of CGA codon repeats in yeast involves quality control components and ribosomal protein L1. *RNA* **19**, 1208-1217 (2013).
25. Brown, A., Baird, M.R., Yip, M.C., Murray, J. & Shao, S. Structures of translationally inactive mammalian ribosomes. *Elife* **7**(2018).
26. Dimitrova, L.N., Kuroha, K., Tatematsu, T. & Inada, T. Nascent peptide-dependent translation arrest leads to Not4p-mediated protein degradation by the proteasome. *J Biol Chem* **284**, 10343-52 (2009).
27. Wilson, D.N. & Beckmann, R. The ribosomal tunnel as a functional environment for nascent polypeptide folding and translational stalling. *Curr Opin Struct Biol* **21**, 274-82 (2011).
28. Chandrasekaran, V. et al. Mechanism of ribosome stalling during translation of a poly(A) tail. *Nat Struct Mol Biol* **26**, 1132-1140 (2019).
29. Sitron, C.S., Park, J.H. & Brandman, O. Asc1, Hel2, and Slh1 couple translation arrest to nascent chain degradation. *RNA* **23**, 798-810 (2017).
30. D'Orazio, K.N. et al. The endonuclease Cue2 cleaves mRNAs at stalled ribosomes during No Go Decay. *Elife* **8**(2019).
31. Ikeuchi, K. et al. Collided ribosomes form a unique structural interface to induce Hel2-driven quality control pathways. *EMBO J* **38**(2019).
32. Sugiyama, T. et al. Sequential Ubiquitination of Ribosomal Protein uS3 Triggers the Degradation of Non-functional 18S rRNA. *Cell Rep* **26**, 3400-3415 e7 (2019).
33. Brandman, O. & Hegde, R.S. Ribosome-associated protein quality control. *Nature Structural & Molecular Biology* **23**, 7-15 (2016).
34. Brandman, O. et al. A ribosome-bound quality control complex triggers degradation of nascent peptides and signals translation stress. *Cell* **151**, 1042-54 (2012).
35. Joazeiro, C.A.P. Mechanisms and functions of ribosome-associated protein quality control. *Nat Rev Mol Cell Biol* (2019).
36. Shen, P.S. et al. Rqc2p and 60S ribosomal subunits mediate mRNA-independent elongation of nascent chains. *Science* **347**, 75-78 (2015).
37. Decourty, L. et al. Linking functionally related genes by sensitive and quantitative characterization of genetic interaction profiles. *Proc Natl Acad Sci U S A* **105**, 5821-6 (2008).
38. Daugeron, M.C., Prouteau, M., Lacroute, F. & Seraphin, B. The highly conserved eukaryotic DRG factors are required for efficient translation in a manner redundant with the putative RNA helicase Slh1. *Nucleic Acids Res* **39**, 2221-33 (2010).
39. Lu, L., Lv, Y., Dong, J., Hu, S. & Peng, R. DRG1 is a potential oncogene in lung adenocarcinoma and promotes tumor progression via spindle checkpoint signaling regulation. *Oncotarget* **7**, 72795-72806 (2016).
40. Schellhaus, A.K. et al. Developmentally Regulated GTP binding protein 1 (DRG1) controls microtubule dynamics. *Sci Rep* **7**, 9996 (2017).

41. Huang da, W., Sherman, B.T. & Lempicki, R.A. Bioinformatics enrichment tools: paths toward the comprehensive functional analysis of large gene lists. *Nucleic Acids Res* **37**, 1-13 (2009).
42. Bailey, T.L. et al. MEME SUITE: tools for motif discovery and searching. *Nucleic Acids Res* **37**, W202-8 (2009).
43. Baudin, A., Ozier-Kalogeropoulos, O., Denouel, A., Lacroute, F. & Cullin, C. A simple and efficient method for direct gene deletion in Saccharomyces cerevisiae. *Nucleic Acids Res* **21**, 3329-30 (1993).
44. Longtine, M.S. et al. Additional modules for versatile and economical PCR-based gene deletion and modification in Saccharomyces cerevisiae. *Yeast* **14**, 953-61 (1998).
45. Jin, H., Kelley, A.C., Loakes, D. & Ramakrishnan, V. Structure of the 70S ribosome bound to release factor 2 and a substrate analog provides insights into catalysis of peptide release. *Proc Natl Acad Sci U S A* **107**, 8593-8 (2010).
46. Zeng, F. & Jin, H. Peptide release promoted by methylated RF2 and ArfA in nonstop translation is achieved by an induced-fit mechanism. *RNA* **22**, 49-60 (2016).
47. Acker, M.G., Kolitz, S.E., Mitchell, S.F., Nanda, J.S. & Lorsch, J.R. Reconstitution of yeast translation initiation. *Methods Enzymol* **430**, 111-45 (2007).
48. Brandariz-Nunez, A., Zeng, F., Lam, Q.N. & Jin, H. Sbp1 modulates the translation of Pab1 mRNA in a poly(A)- and RGG-dependent manner. *RNA* **24**, 43-55 (2018).
49. Regulski, E.E. & Breaker, R.R. In-line probing analysis of riboswitches. *Methods Mol Biol* **419**, 53-67 (2008).
50. Xu, X., Lambrecht, A.D. & Xiao, W. Yeast survival and growth assays. *Methods Mol Biol* **1163**, 183-91 (2014).
51. Pelechano, V., Wei, W. & Steinmetz, L.M. Genome-wide quantification of 5'-phosphorylated mRNA degradation intermediates for analysis of ribosome dynamics. *Nat Protoc* **11**, 359-76 (2016).
52. Martin, M. Cutadapt removes adapter sequences from high-throughput sequencing reads. *2011* **17**, 3 (2011).
53. Langmead, B., Trapnell, C., Pop, M. & Salzberg, S.L. Ultrafast and memory-efficient alignment of short DNA sequences to the human genome. *Genome Biol* **10**, R25 (2009).
54. Langmead, B. & Salzberg, S.L. Fast gapped-read alignment with Bowtie 2. *Nat Methods* **9**, 357-9 (2012).
55. Zeng, F. et al. Structural basis of co-translational quality control by ArfA and RF2 bound to ribosome. *Nature* **541**, 554-557 (2017).
56. Zheng, S.Q. et al. MotionCor2: anisotropic correction of beam-induced motion for improved cryo-electron microscopy. *Nat Methods* **14**, 331-332 (2017).
57. Rohou, A. & Grigorieff, N. CTFFIND4: Fast and accurate defocus estimation from electron micrographs. *J Struct Biol* **192**, 216-21 (2015).
58. Zivanov, J. et al. New tools for automated high-resolution cryo-EM structure determination in RELION-3. *Elife* **7**(2018).
59. Pettersen, E.F. et al. UCSF Chimera--a visualization system for exploratory research and analysis. *J Comput Chem* **25**, 1605-12 (2004).
60. Schrodinger, LLC. The PyMOL Molecular Graphics System, Version 1.8. (2015).

61. Scheres, S.H. & Chen, S. Prevention of overfitting in cryo-EM structure determination. *Nat Methods* **9**, 853-4 (2012).